catalysts

MDPI

Article

Reduced Graphene Oxide-Supported Pt-Based Catalysts for PEM Fuel Cells with Enhanced Activity and Stability

Irina V. Pushkareva [1,2], Artem S. Pushkarev [1,2,3], Valery N. Kalinichenko [2,4,5], Ratibor G. Chumakov [2,3], Maksim A. Soloviev [1,2], Yanyu Liang [6], Pierre Millet [7] and Sergey A. Grigoriev [1,2,8,*]

1 National Research University "Moscow Power Engineering Institute", 14, Krasnokazarmennaya st., 111250 Moscow, Russia; PushkarevaIV@mpei.ru (I.V.P.); PushkarevAS@mpei.ru (A.S.P.); SolovyevMaxA@mpei.ru (M.A.S.)
2 National Research Center "Kurchatov Institute", 1, Akademika Kurchatova sq., 123182 Moscow, Russia; kalinval47@mail.ru (V.N.K.); Chumakov_RG@nrcki.ru (R.G.C.)
3 Moscow Institute of Physics and Technology, 9, Institutskiy per., Dolgoprudny, 141701 Moscow Region, Russia
4 N.N. Semenov Federal Research Center for Chemical Physics, Russian Academy of Sciences, 119991 Moscow, Russia
5 N.M. Emanuel Institute of Biochemical Physics, Russian Academy of Sciences, 119991 Moscow, Russia
6 College of Materials Science and Technology, Nanjing University of Aeronautics and Astronautics, Nanjing 211106, China; liangyy403@126.com
7 Institut de Chimie Moléculaire et des Matériaux d'Orsay, Université Paris-Saclay, 91405 Orsay, France; pierre.millet@universite-paris-saclay.fr
8 HySA Infrastructure Center of Competence, Faculty of Engineering, North-West University, Potchefstroom 2531, South Africa
* Correspondence: grigoryevsa@mpei.ru or sergey.grigoriev@outlook.com

Citation: Pushkareva, I.V.; Pushkarev, A.S.; Kalinichenko, V.N.; Chumakov, R.G.; Soloviev, M.A.; Liang, Y.; Millet, P.; Grigoriev, S.A. Reduced Graphene Oxide-Supported Pt-Based Catalysts for PEM Fuel Cells with Enhanced Activity and Stability. *Catalysts* **2021**, *11*, 256. https://doi.org/10.3390/catal11020256

Academic Editor: Vincenzo Baglio
Received: 24 January 2021
Accepted: 8 February 2021
Published: 15 February 2021

Abstract: Platinum (Pt)-based electrocatalysts supported by reduced graphene oxide (RGO) were synthesized using two different methods, namely: (i) a conventional two-step polyol process using RGO as the substrate, and (ii) a modified polyol process implicating the simultaneous reduction of a Pt nanoparticle precursor and graphene oxide (GO). The structure, morphology, and electrochemical performances of the obtained Pt/RGO catalysts were studied and compared with a reference Pt/carbon black Vulcan XC-72 (C) sample. It was shown that the Pt/RGO obtained by the optimized simultaneous reduction process had higher Pt utilization and electrochemically active surface area (EASA) values, and a better performance stability. The use of this catalyst at the cathode of a proton exchange membrane fuel cell (PEMFC) led to an increase in its maximum power density of up to 17%, and significantly enhanced its performance especially at high current densities. It is possible to conclude that the optimized synthesis procedure allows for a more uniform distribution of the Pt nanoparticles and ensures better binding of the particles to the surface of the support. The advantages of Pt/RGO synthesized in this way over conventional Pt/C are the high electrical conductivity and specific surface area provided by RGO, as well as a reduction in the percolation limit of the components of the electrocatalytic layer due to the high aspect ratio of RGO.

Keywords: graphene; graphene oxide; reduced graphene oxide; polymer electrolyte membrane fuel cell; catalyst support; catalytic layer; platinum; platinum utilization

1. Introduction

Platinum (Pt)-based electrocatalysts are commonly used in proton exchange membrane fuel cells (PEMFCs). The platinum nanoparticles must be dispersed uniformly on the surface of a suitable support (catalyst carrier) in order to maximize the active surface and the catalytic activity, to improve the stability, and to reduce the cost of electrodes [1]. Carbon blacks (Vulcan XC-72, Ketjen Black, etc.), which have the merit of being easily

available and inexpensive, are commonly used as supports for electrocatalysts in PEMFCs [2]. However, they contain deep micropores (up to 47% [3]) that reduce the flow of reagents and are poorly connected, which affects the electrical conductivity of the support. In addition, Pt nanoparticles may be trapped into micropores, with no access to ionomer and reagents, and this can decrease the electrochemically active surface area (EASA) of the catalyst [4]. The presence of impurities and poor stability are other major disadvantages; the latter directly affects the durability of the catalytic layers—carbon corrosion accelerates the detachment or agglomeration of Pt nanoparticles [5,6] and increases oxygen transport resistance in the catalytic layer [7].

The performance of carbon black-based catalytic layers can be improved through the addition of functional additives such as carbon nanotubes (CNTs) [8] or reduced graphene oxide (RGO) [9,10], especially at high current densities [11]. For instance, RGO nanoplatelets act as spacers between the platinized carbon black agglomerates, decreasing the catalytic layer percolation threshold (electronic conductivity) [12] and enhancing mass transfer [11]. Carbon black durability could be increased, for example, through the preparation of composites with stable oxides [13,14] or using any heteroatom doping approaches [15]. Several alternatives, such as carbon nanotubes [16], nanofibers [17], mesoporous carbons [18], and graphene-based materials [19–23], have been considered.

The key advantages of graphene-based materials are their high specific surface, chemical stability, and graphitic structure [24] (providing high electrochemical durability); superior electronic conductivity; and strong metal–support interaction, which stabilize Pt nanoparticles from growth and leaching [25,26]. Their layered structure may enhance the catalyst layer mass transfer [27]. On the other hand, layered graphene-based materials are prone to restack because of Van-der-Waals interactions and the tendency of nanosheets to agglomerate in aqueous solutions [28,29], which may be suppressed.

The method of colloidal reduction/deposition of Pt nanoparticles is often used because of its simplicity and the possibility of implementing it on a large scale [30]. Different synthetic approaches have been proposed in the literature to obtain Pt/RGO catalysts [31–36]. The research of Sanli et al. [32] showed that the colloidal reduction in ethylene glycol (EG) could yield a Pt/RGO catalyst with a high activity and uniformly distributed small nanoparticles when compared with sodium borohydride and ascorbic acid reductions. On the other hand, polyol synthesis is sensitive to various experimental parameters and procedures. According to the authors of [30], the process pH, the type of Pt precursor, and the OH^-/Pt ratio are parameters of great importance; the use of $H_2PtCl_6 \cdot 6H_2O$ and alkali media (pH = 12) in one-pot polyol synthesis were considered. Moreover, the simultaneous polyol reduction has several advantages over consecutive methods (separate reduction of GO and Pt nanoparticles)—GO is able to form well-dispersed colloids because of the electrostatic repulsion of oxygen-containing functional groups [37], which can also serve as additional sites for Pt nanoparticle binding [38]. Pt nanoparticles not only promote the catalytic reduction of GO, but also prevent the agglomeration and "restacking" of sheets ("flakes") of RGO [39].

Most of the proposed methods are focused on low-Pt-loaded catalysts (up to 20 wt.%) with small Pt nanoparticles, which could be unstable [40], whereas the optimal (balanced in terms of activity and durability) size is considered to be ca. 4–5 nm [41]. The PEMFC membrane electrode assembly (MEA) performance significantly depends on not only on the activity and EASA of the catalysts, but also on the catalytic layer structure and thickness. For instance, a thinner catalytic layer (with a higher Pt content) provides a better mass transfer and lower charge transfer resistance within the active layer [42–44]. Layers with a Pt content gradient structure have also been proposed [45].

The proposed study focused on RGO-supported catalysts with a relatively high Pt content forming thinner catalytic layers (considering the same cathode Pt loading), favorable for applications in H_2/O_2 (air) PEMFC. A modified polyol approach using ethylene glycol and formaldehyde as reductants was developed to obtain RGO-supported catalysts; it includes the simultaneous "one-pot" reduction of both Pt nanoparticles and RGO precursors. The obtained Pt/RGO(s) catalysts were characterized using different

techniques, including X-ray diffraction (XRD) and X-ray photoemission spectroscopy (XPS), transmission electron microscopy (TEM), cyclic voltammetry and accelerated stress testing (AST) in comparison with the Pt/carbon black Vulcan XC-72 (C) and Pt/RGO catalysts obtained conventionally. Finally, the obtained catalysts were implemented at the cathodes of the H_2/O_2 PEMFC MEAs and tested.

2. Results and Discussion

The structure and morphology of the Pt/C, Pt/RGO, and Pt/RGO(s) catalysts were determined through TEM analysis. Figure 1 shows that instead of some agglomeration, the Pt nanoparticles of all of the studied catalysts were quite small and finely dispersed over the surface of the carbon substrate. Their size distributions (see insets of Figure 1) were obtained using the well-known ImageJ software [46]. The analysis was based on no less than 100 particles for each catalyst. The size of most Pt nanoparticles (ca. 80%) was between 3 and 5 nm. The mean particle sizes of the Pt/C, Pt/RGO, and Pt/RGO(s) catalysts were 3.6, 3.9, and 3.95 nm, respectively. Particle agglomeration made it difficult to precisely evaluate the nanoparticle size, thus XRD analysis was used to find the Pt crystallite size (see below).

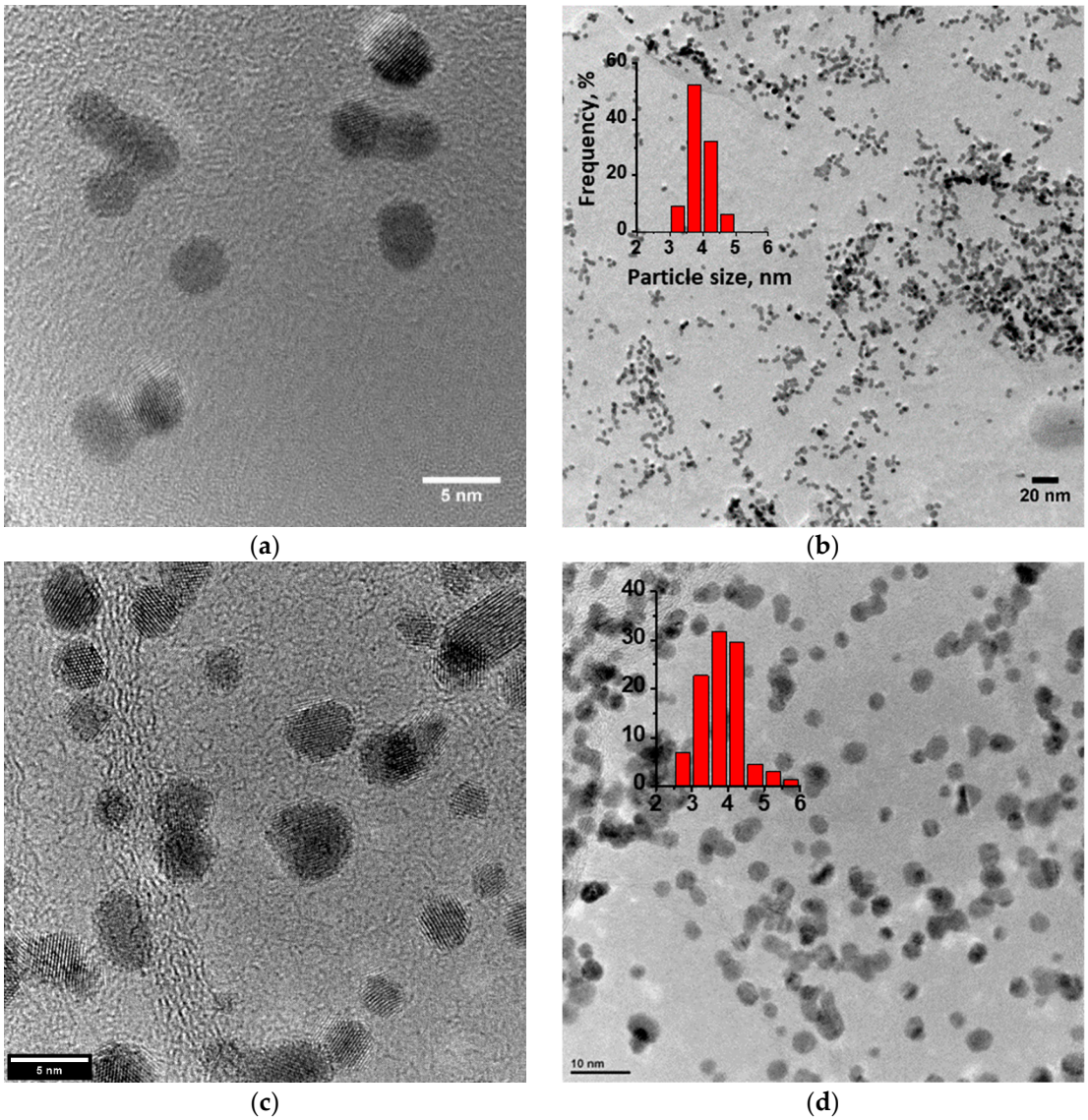

Figure 1. *Cont.*

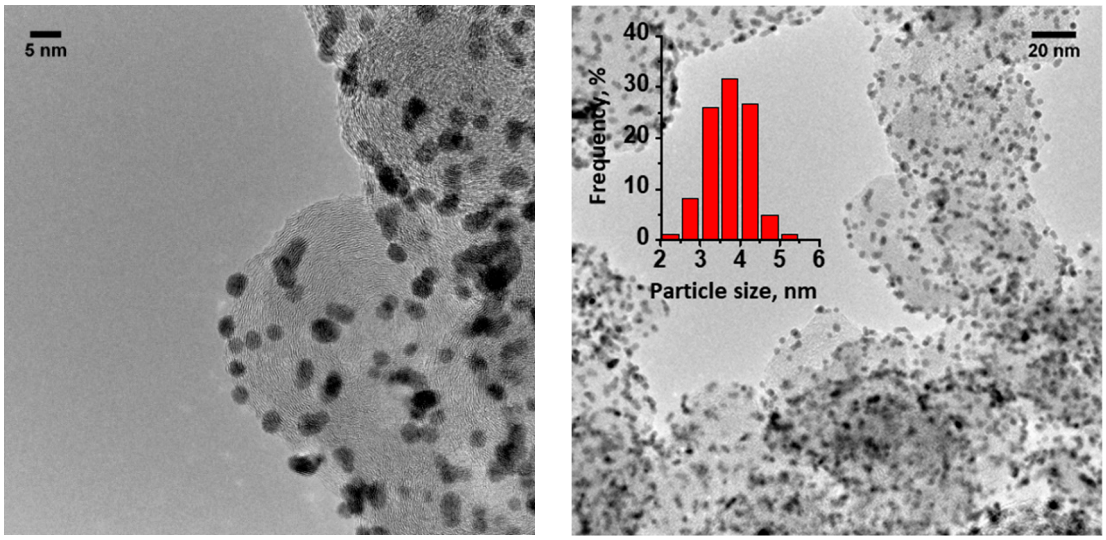

Figure 1. TEM images of different catalysts: (**a**,**b**) Pt/reduced graphene oxide(s) (RGO(s)) (s), (**c**,**d**) Pt/RGO, and (**e**,**f**) Pt/carbon black Vulcan XC-72 (C), as well as Pt nanoparticles' size distribution (see insets).

The reduction of GO led to significant structure changes. The XRD spectra of exfoliated GO usually shows an intensive (001) peak with an interplane distance of ca. 7.4 Å [47], which is higher than graphite interplane distance (3.37 Å), and because of the various functional groups formed and C–C bonds disruption during the oxidation [32] (see XPS spectra given below). The XRD spectra of RGO (Figure 2) exhibited a main peak at 2θ = 30.5°, corresponding to the (002) plane with an interplane distance of ca. 3.4 Å, suggesting the partial restoration of the graphitic structure.

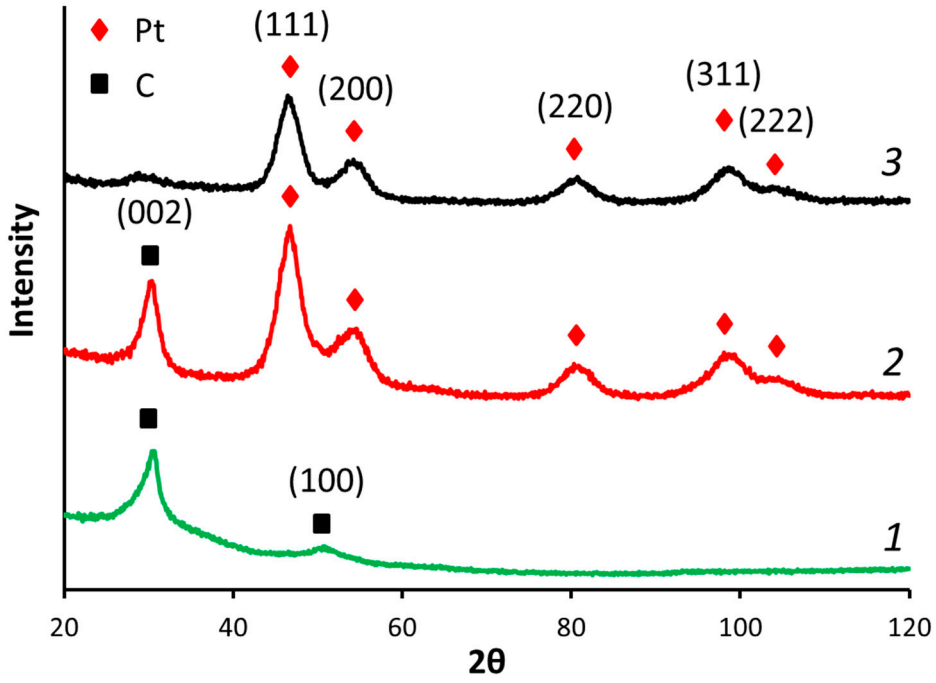

Figure 2. XRD spectra of (1) RGO, (2) Pt/RGO(s), and (3) Pt/C.

The XRD spectra of the Pt/RGO(s) and Pt^{40}/C catalysts are shown in Figure 2. They exhibited clear peaks located at 46.7°, 54.0°, 80.8°, and 98.6°, corresponding to the (111), (200), (220), and (311) planes, respectively, of the face-centered cubic lattice of Pt (JCPDS No.

4-802, considering the Co Kα source being used here). The spectra of Pt/RGO(s) (Figure 2) shows the (002) peak of carbon at 30.7° considering the multilayered RGO support [48,49]. The Scherrer equation was used to calculate the mean size of the Pt crystallites, as follows:

$$d_{XRD} = \frac{K\lambda}{\beta \cos\theta_\beta} \quad (1)$$

where d_{XRD} is the mean size of the Pt crystallites (in nm), K is the Scherrer constant (for spherical particles with cubic symmetry this is equal to 0.94), λ is the Co Kα radiation wavelength (0.178897 nm), β is the full peak width at half maximum (rad), and θ_β is the Bragg angle (degrees).

The mean sizes of the Pt crystallites of Pt/C, Pt/RGO, and Pt/RGO(s) were ca. 3.60, 3.55, and 3.50 nm, respectively. It should be mentioned that the mean size of the RGO-supported Pt nanoparticles is slightly higher in comparison with the Vulcan XC-72 supported ones, possibly because of some agglomeration of RGO during its reduction (thermal or chemical) [39]. The simultaneous reduction of precursors did not significantly affect the mean Pt crystallite size (measured by XRD) or the mean nanoparticles size (d_{TEM}) deduced from the analysis of the TEM images (see combined Pt crystallites/nanoparticles sizes data in Table 1).

Table 1. Comparative parameters of the obtained catalysts.

Catalyst	d_{XRD}, nm	d_{TEM}, nm	EASA, $m^2\ g^{-1}$ Pt	S_{Pt}, $m^2\ g^{-1}$ Pt [1]	u_{Pt}, %
Pt/C	3.5	3.60	79.0	54	68.3
Pt/RGO	3.9	3.55	75.2	48	63.8
Pt/RGO(s)	3.95	3.50	75.2	60	79.8

[1] Calculated using the mean value of the Pt nanoparticles size taken between d_{XRD} and d_{TEM}.

CasaXPS software [50] was used to analyze the experimental data and decompose the lines into constituent components. The Gaussian–Lorentzian sum functions were used to interpret the spectra of the individual lines. The National Institute of Standards and Technology (NIST) laboratory database was used to determine the positions and shapes of the lines [51]. According to the C 1s spectra (Figure 3a–c), RGO-supported catalysts primarily consist of sp^2–carbon (at ca. 284.5 eV). The sp^2/sp^3 ratios of Pt/C, Pt/RGO, and Pt/RGO(s) were 1.27, 36.2, and 38.6, respectively, suggesting that the graphitic structure of RGO-supported catalysts was successfully restored during GO reduction using both approaches—thermal reduction and simultaneous polyol reduction. Moreover, their C/O ratio values were close, and were equal to ca. 9.5. At a low binding energy, the spectra showed a few peak duplets (Figure 3d–f) corresponding to Pt at different oxidation states. To distinguish the metallic Pt(0), Pt(II) ($PtO/Pt(OH)_2$), and Pt (IV) (PtO_2), the obtained spectra were deconvoluted into a series of Pt $4f_{7/2}$ and $4f_{5/2}$ doublets, with a fixed ratio for the intensity and energy shift [52]. The obtained spectra suggest that Pt(0) is the predominant oxidation state in all catalysts (ca. 47–55%). On the other hand, all of the samples presented a variable amount of Pt(II) and Pt(IV) species deduced from the Pt $4f_{7/2}$ peaks at binding energy values of ca. 72–75 eV, which could be attributed to the partial surface oxidation of small Pt metal nanoparticles [53]. The Pt(0) content of Pt/C, Pt/RGO, and Pt/RGO(s) were ca. 46.7, 43.2, and 55.2%, respectively. The lower amount of oxidized Pt in the case of Pt/RGO(s) could be explained by the particle size effect (smaller nanoparticles have more surface atoms, which are prone to oxidize) [53] or by the residual Pt(II) and Pt(IV) species from the polyol reduction process, in which Pt (IV) reduced to Pt (II) and then reached the metallic form [54]. It is worth noting that the Pt(0) surface provided an active site for electrochemical reactions, but not the Pt(II) and Pt(IV) species.

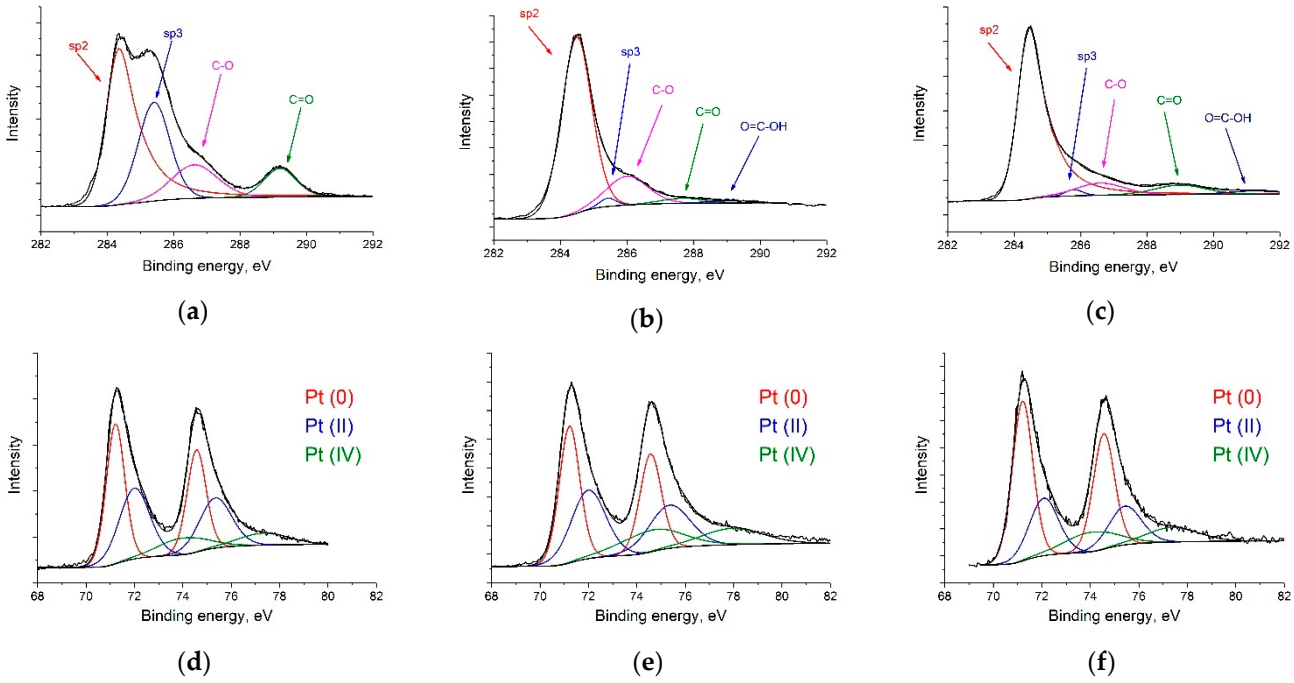

Figure 3. XPS spectra of (**a**,**d**) Pt/C, (**b**,**e**) Pt/RGO, and (**c**,**f**) Pt/RGO(s).

The cyclic voltammograms of the different catalysts recorded under an N_2-purged 1M H_2SO_4 solution are shown in Figure 4. Well-defined hydrogen adsorption/desorption and oxygenated species adsorption/desorption peaks, typical of Pt-based catalysts [55], were observed for the studied catalysts at −0.15–0.20 and 0.6–0.8 V, respectively, vs. the Ag/AgCl reference electrode. The electrochemical active surface areas (EASAs) of Pt^{40}/C, Pt^{40}/RGO, and Pt^{40}/RGO(s) were ca. 54, 48, and 60 m^2 Pt g^{-1}, respectively. These values are in agreement with the data reported in the literature [32,35,56] for RGO-supported catalysts of a similar Pt percentage and Pt nanoparticles size.

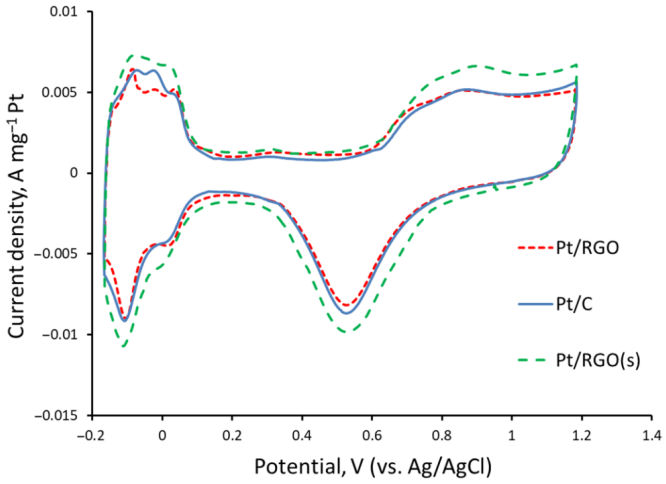

Figure 4. Cyclic voltammograms of Pt^{40}/C, Pt^{40}/RGO, and Pt^{40}/RGO(s) measured in an N_2-purged 1M H_2SO_4 solution at 20 mV s^{-1}.

The accessibility of the Pt nanoparticles and the catalytic layer connectivity could be analyzed using the Pt utilization value. One hundred percent Pt utilization means that all Pt nanoparticles were integrated into the entire electron conductivity network, and were

fully accessible by the electrolyte. The approximate value of the full surface area of the Pt nanoparticles can be calculated according to the following equation [57,58]:

$$S_{Pt} = \frac{6000}{\rho \cdot d} \quad (2)$$

where S_{Pt} is the total surface of Pt ($m^2\ g^{-1}$ Pt), ρ is the bulk Pt density (21.4 g cm^{-3}), and d is the Pt nanoparticles mean size (nm; taken as the mean value between d_{XRD} and d_{TEM}). Thus, the Pt utilization (u_{Pt}, %) can be calculated as an EASA divided by the total surface area of Pt, as follows:

$$u_{Pt} = \frac{\text{EASA}}{S_{Pt}} \cdot 100 \quad (3)$$

The values of d_{XRD}, d_{TEM}, EASA, S_{Pt}, and u_{Pt} are collected in Table 1.

The obtained EASA values were lower than the values of the total area of the Pt calculated from Equation (2), because of the different use of Pt, which was generally less than 100%, even when the catalytic films that were used were thin. For instance, the u_{Pt} value of a commercial E-TEK catalyst (with 20 wt.% of Pt) was 68% [59]. When graphene-based materials were used as a substrate, the Pt utilization of a catalyst strongly depended on the synthesis procedure, type of precursors, etc. [30,32,35]. According to the results of Sanli et al. [32], the u_{Pt} of various RGO-supported catalysts prepared using different approaches could vary from 28 to 93%. Here, ethylene glycol (EG), simultaneously acting as a reductant, stabilizer, and dispersing agent [32], could form small and uniformly distributed Pt nanoparticles. Moreover, the use of RGO as a support, together with the simultaneous reduction approach, allowed for decreasing the agglomeration of particles and increasing the Pt utilization in Pt^{40}/RGO(s). On the other hand, the stability of the obtained catalysts is another important factor that should be also considered. Figure 5 shows the variation of the EASA of the catalysts during AST.

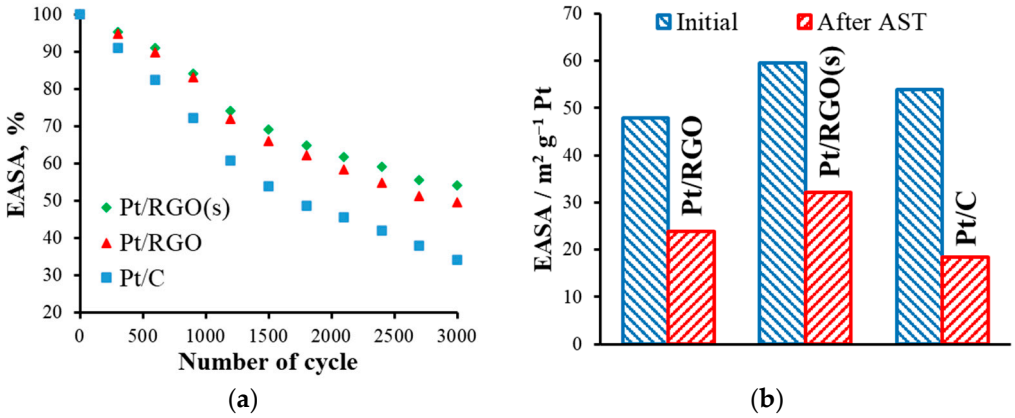

(**a**) (**b**)

Figure 5. (**a**) The effect of the accelerated stress testing (AST) cycles on the catalysts' electrochemically active surface area (EASA) values, and (**b**) a comparison of the initial and aged catalysts' EASA values.

The EASA of all of the catalysts studied decreased significantly during AST. The main degradation mechanisms included (i) electrochemical Ostwald ripening, (ii) particle migration and coalescence, (iii) detachment from carbon support (mainly from carbon corrosion), and (iv) platinum dissolution and re-precipitation inside the ionomer phase [60–66]. As the initial particle size of the Pt nanoparticles of the different catalysts studied was similar, their different stability could be mainly attributed to the type of carbon support used. Moreover, corrosion of the carbon support was expected to be the prevailing degradation mechanism because of the potential range selected for the AST procedure [13]. After 3000 AST cycles, the EASA residual values of Pt/C, Pt/RGO, and Pt/RGO(s) were 18.4, 23.8, and 32.1 $m^2\ g^{-1}$ Pt, or 34, 49.5, and 53.9%, respectively. It is important to note that the electronic interactions between the Pt nanoparticles and graphene support could be

responsible for the higher durability observed in the RGO-supported catalysts, as discussed in the literature [67]. Such enhanced metal–substrate interactions are evidenced by the negative shift in the Pt 4f binding energy on the XPS spectra [68], suggesting that electrons were transferred from the respective carbon supports to Pt. However, both RGO-supported catalysts showed a higher durability in comparison with Pt/C. A possible explanation is the hindered corrosion of the RGO support itself as a result of the smaller number of disordered sites in comparison with carbon black. Such disordered domains (sp^3 hybridized) are prone to be oxidized first at a high rate compared with the ordered sp^2 graphitic structure of RGO [69,70].

After characterization, the different catalysts (Pt/C, Pt/RGO, and Pt/RGO(s)) were studied as cathode catalysts in H_2/O_2 PEMFC. The voltage and power density vs. current density are shown in Figure 6.

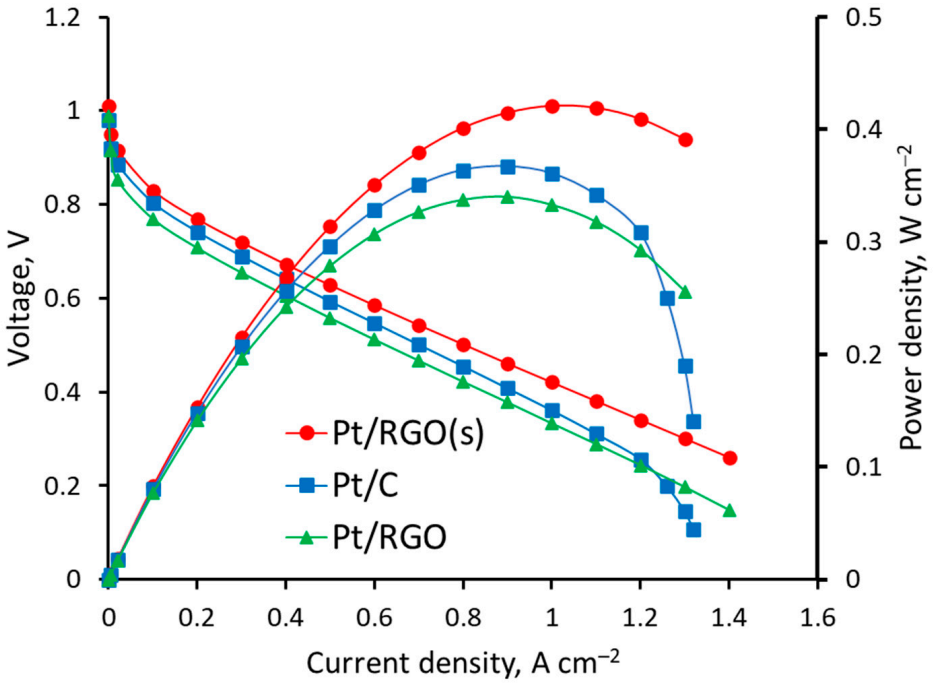

Figure 6. Voltage and power density vs. current density curves of H_2/O_2 proton exchange membrane fuel cells (PEMFCs) measured at 1 bar gauge pressure at 60 °C and 1.5 gas stoichiometry.

According to Figure 6, the cell voltages measured at 0.5 A cm^{-2} on the PEMFC with Pt/C, Pt/RGO, and Pt/RGO(s) were ca. 0.593, 0.558, and 0.628 V, respectively. The use of RGO as a catalyst support, regardless of the technique used for the deposition of Pt nanoparticles, provided a better MEA performance at high current densities >1.2 A cm^{-2} because of the better reagents/products mass transfer in the cathode catalyst layer [71]. Significant mass transfer limitations were observed at high current densities with the Pt/C-based MEA (Figure 6), while the polarization curves of Pt/RGO and Pt/RGO(s) remained linear up to 1.4 A cm^{-2}. The worse performance of Pt/RGO-based MEA could be ascribed to the lower catalyst EASA and Pt utilization discussed earlier, due to the agglomeration of RGO (during the catalyst synthesis and the catalyst deposition over the gas diffusion electrode (GDE) [21]); however, the open layered structure of RGO allowed for sustaining high current densities without significant transport limitations [12,72]. This suggestion is in good agreement with the results described in the literature [30], according to which the wrinkled sheet-like structure of RGO is superior to carbon black in terms of providing gas flow channels and a high accessibility for the reactant gases. The high aspect ratio of RGO allowed for reducing the percolation limits [72] of the electrocatalytic layer's components responsible for mass, electron, and proton transport.

The maximum power densities measured on PEMFC MEAs containing Pt/C, Pt/RGO, and Pt/RGO(s) were ca. 0.358, 0.337, and 0.421 W cm^{-2}, respectively. The simultaneous reduction of Pt and RGO precursors during synthesis provided a significantly better PEMFC MEA performance. This was mainly due to the higher catalyst EASA, higher Pt utilization, and less agglomerated support structure, which provided effective mass transport of the oxygen reduction reaction reagents and products. The sorption of H_2PtCl_6 by the GO surface and its further simultaneous reduction were possibly responsible for the narrow and uniform Pt nanoparticles distribution over the RGO surface. The Pt nanoparticles nucleated during the synthesis might have enhanced the dispersibility of the RGO and prevent restacking, thus providing a high EASA and Pt utilization.

3. Materials and Methods

3.1. Preparation of Catalysts

Preparation of the Pt/C (C—carbon black Vulcan XC-72, purchased from Cabot Corporation, Boston, MA, USA) and Pt/RGO electrocatalysts (40 wt.% of Pt) was carried out using a modified polyol synthesis procedure, in which the reduction of the Pt precursor (H_2PtCl_6 $2H_2O$) was performed using ethylene glycol and formaldehyde as reductants, according to the literature [73]. The RGO support were obtained through the thermal reduction of GO obtained by modified Hummers' method, as described in the literature [9,10]. Pt^{40}/RGO(s) were obtained by the same procedure, but with the addition of GO instead of carbon support, i.e., GO and Pt nanoparticles precursor were reduced "in one pot" in order to obtain the Pt/RGO(s) catalyst.

3.2. Structural and Morphological Studies

The XRD studies were performed using a D8 Advance diffractometer (Bruker, Billerica, MA, USA), using Co Kα radiation at 2θ = 20–120° with a step of Δ2θ = 0.07°. A scanning/transmission electron microscope, Titan 80–300 (Thermo-Fisher Scientific, Beverly, MA, USA), equipped with an energy dispersive X-ray spectrometer (EDAX, Mahwah, NJ, USA) was used to study the morphology of the catalysts. The XPS studies were performed using a PHOIBOS 150 (SPECS Surface Nano Analysis GmbH, Berlin, Germany) hemispherical analyzer and monochromatic Al Kα radiation, with a photon energy of 1486.61 eV and an end resolution of ΔE = 0.2 eV, located at the facility of the Kurchatov Complex of Synchrotron and Neutron Investigation (NRC "Kurchatov Institute", Moscow, Russian Federation). The powdered samples were pressed into carbon scotch tape and were transferred to the vacuum chamber of a spectrometer with a base pressure of 3×10^{-9} mbar. All of the spectra were measured in fixed analyzer transmission mode, with a pass energy of 120 and 40 eV for the survey spectra and separated lines, respectively. To analyze the experimental data and decompose the lines into constituent components, CasaXPS software (v. 2.3.23, Casa Software Ltd., Teignmouth, UK) was used [50]. The NIST laboratory database (v. 4.1, National Institute of Standards and Technology, Gaithersburg, MD, USA) was used to determine the position of the lines [52].

3.3. Electrochemical Studies

Electrochemical studies were carried out using a Solartron 1280 (AMETEK, Inc., Berwyn, PA, USA), with thin catalytic films formed on the surface of the glassy carbon disk working electrodes, according to the previously described procedures [13,74,75]. Briefly, the EASA of the catalysts were determined from their CVs measured in deaerated 1 M H_2SO_4 at 25 °C with a 20 mV/s sweep rate. The charges associated with the adsorption/desorption of hydrogen monolayers were taken to calculate the EASA (m^2/g Pt) [74,76]. ASTs aimed at studying the impact of the corrosion of the support on the durability of the electrochemical performances were performed using an approach described earlier [13]. In brief, thin catalytic films were formed (as described above), and the working electrodes were subjected to potential cycling from 0.8 to 1.4 V vs. reversible hydrogen electrode at 0.1 V s^{-1} in an oxygen purged 1 M H_2SO_4 solution.

3.4. Fuel Cell MEAs Fabrication and Testing

PEM fuel cell MEAs were prepared using Nafion® 115 (DuPont Inc., Wilmington, DE, USA) as the polymer electrolyte membrane and Sigracet 39BC (SGL Group GmbH, Wiesbaden, Germany) as the anode and cathode GDEs. Pt^{40}/C was used as the anode catalyst. The synthesized Pt/C, Pt/RGO, and Pt/RGO(s) materials were used as the cathode catalysts. The Pt loading of the anode and cathode electrocatalytic layers were 0.2 and 0.4 mg cm^{-2}, respectively. Catalytic layers were formed on the GDE surface by air-spraying catalytic ink containing 15 wt.% Nafion® ionomer (Ion Power, Navarre, FL, USA), as described in the literature [20]. The MEA components were clamped in a circular titanium test cell with an active area of 7 cm^2, as described elsewhere [12,20,77], and were kept at 90 °C for 2 h to ensure the tight binding of the MEA components. Such mild manufacturing conditions prevented the damage to the porous structure (the GDE and its microporous sublayer), which could be caused by any type of hot-press approach and ensured a high MEA performance at high current densities [78,79]. MEA testing was carried out using pure hydrogen and oxygen at a relative humidity of 100%, cell temperature of 60 °C, and at a bar gauge gas pressure of 1.

4. Conclusions

RGO-supported electrocatalysts designed for operation at the cathode of PEMFCs were synthesized using both the conventional two-step polyol process, and the simultaneous reduction of the Pt precursor and GO during a modified polyol process with EG and formaldehyde as the synthesis environment/reducing agents. The Pt/RGO(s) obtained by the optimized simultaneous reduction process showed high Pt utilization and EASA values, and a better durability during AST, provoking strong oxidation of the carbon support. The benefits of Pt/RGO(s) in comparison with conventionally prepared Pt/RGO and Pt/C are suggested to be as a result of the hindered RGO agglomeration during synthesis, optimized Pt nanoparticles morphology, and the ordered sp^2 graphitic structure of RGO. The implementation of the synthesized Pt/RGO(s) material as a cathode catalyst in H_2/O_2 PEMFC allowed for increasing the maximum power density by up to 17% and to significantly enhance its performance, especially at high current densities.

Author Contributions: Conceptualization, I.V.P. and A.S.P.; methodology, I.V.P., A.S.P., and R.G.C.; validation, I.V.P., A.S.P., and V.N.K.; investigation, I.V.P., M.A.S., and V.N.K.; resources, S.A.G.; writing—original draft preparation, I.V.P. and A.S.P.; writing—review and editing, Y.L., P.M., and S.A.G.; visualization, A.S.P. and I.V.P.; supervision, S.A.G.; project administration, S.A.G. and A.S.P.; funding acquisition, S.A.G. and A.S.P. All authors have read and agreed to the published version of the manuscript.

Funding: This work was partly supported by the scholarship of the President of the Russian Federation to young scientists and graduate students engaged in advanced research in priority areas of Russian economy modernization for 2019–2021 (СП-1764.2019.1), and partly within the framework of the project "Modified carbon nanomaterials for electrodes of fuel cells with solid polymer electrolyte", with the support of a grant from the National Research University "Moscow Power Engineering Institute" for the implementation of scientific research programs "Energy", "Electronics, Radio Engineering and IT", and "Industry 4.0 Technologies for Industry and Robotics in 2020–2022".

Data Availability Statement: The data presented in this study are available on request from the corresponding author.

Acknowledgments: Thanks to M.Yu. Presnyakov for capturing the TEM images, and to E.K. Lyutikova, M.V. Kozlova, and S.I. Butrim for their help with the catalysts synthesis and investigations.

Conflicts of Interest: The authors declare no conflict of interest. The funders had no role in the design of the study; in the collection, analyses or interpretation of data; in the writing of the manuscript; or in the decision to publish the results.

References

1. Antolini, E.; Gonzalez, E.R. Ceramic materials as supports for low-temperature fuel cell catalysts. *Solid State Ion.* **2009**, *180*, 746–763. [CrossRef]
2. Shahgaldi, S.; Hamelin, J. Improved carbon nanostructures as a novel catalyst support in the cathode side of PEMFC: A critical review. *Carbon N. Y.* **2015**, *94*, 705–728. [CrossRef]
3. Dai, L.; Chang, D.W.; Baek, J.B.; Lu, W. Carbon nanomaterials for advanced energy conversion and storage. *Small* **2012**, *8*, 1130–1166. [CrossRef] [PubMed]
4. Trogadas, P.; Fuller, T.F.; Strasser, P. Carbon as catalyst and support for electrochemical energy conversion. *Carbon N. Y.* **2014**. [CrossRef]
5. Yu, Y.; Li, H.; Wang, H.; Yuan, X.-Z.; Wang, G.; Pan, M. A review on performance degradation of proton exchange membrane fuel cells during startup and shutdown processes: Causes, consequences, and mitigation strategies. *J. Power Sources* **2012**, *205*, 10–23. [CrossRef]
6. Mamat, M.S.; Grigoriev, S.A.; Dzhus, K.A.; Grant, D.M.; Walker, G.S. The performance and degradation of Pt electrocatalysts on novel carbon carriers for PEMFC applications. *Int. J. Hydrogen Energy* **2010**, *35*, 7580–7587. [CrossRef]
7. Kneer, A.; Jankovic, J.; Susac, D.; Putz, A.; Wagner, N.; Sabharwal, M.; Secanell, M. Correlation of Changes in Electrochemical and Structural Parameters due to Voltage Cycling Induced Degradation in PEM Fuel Cells. *J. Electrochem. Soc.* **2018**, *165*, F3241–F3250. [CrossRef]
8. Glebova, N.V.; Nechitailov, A.A.; Krasnova, A.O.; Tomasov, A.A.; Zelenina, N.K. Cathode of hydrogen fuel cell, with modified structure and hydrophobicity. *Russ. J. Appl. Chem.* **2015**, *88*, 769–774. [CrossRef]
9. Pushkarev, A.S.; Pushkareva, I.V.; Grigoriev, S.A.; Kalinichenko, V.N.; Presniakov, M.Y.; Fateev, V.N. Electrocatalytic layers modified by reduced graphene oxide for PEM fuel cells. *Int. J. Hydrogen Energy* **2015**, *40*, 14492–14497. [CrossRef]
10. Grigor'ev, S.A.; Pushkarev, A.S.; Kalinichenko, V.N.; Pushkareva, I.V.; Presnyakov, M.Y.; Fateev, V.N. Electrocatalytic layers based on reduced graphene oxide for fabrication of low-temperature fuel cells. *Kinet. Catal.* **2015**, *56*, 689–693. [CrossRef]
11. Sung, C.-C.; Liu, C.-Y.; Cheng, C.C.J. Durability improvement at high current density by graphene networks on PEM fuel cell. *Int. J. Hydrogen Energy* **2014**, *39*, 11706–11712. [CrossRef]
12. Baranov, I.E.; Nikolaev, I.I.; Pushkarev, A.S.; Pushkareva, I.V.; Kalinnikov, A.A.; Fateev, V.N. Numerical Modeling of Polymer Electrolyte Fuel Cell Catalyst Layer with Different Carbon Supports. *Int. J. Electrochem. Sci.* **2018**, *13*, 8673–8685. [CrossRef]
13. Spasov, D.D.; Ivanova, N.A.; Pushkarev, A.S.; Pushkareva, I.V.; Presnyakova, N.N.; Chumakov, R.G.; Presnyakov, M.Y.; Grigoriev, S.A.; Fateev, V.N. On the influence of composition and structure of carbon-supported Pt-SnO_2 hetero-clusters onto their electrocatalytic activity and durability in PEMFC. *Catalysts* **2019**, *9*. [CrossRef]
14. Labbé, F.; Disa, E.; Ahmad, Y.; Guérin, K.; Asset, T.; Maillard, F.; Chatenet, M.; Metkemeijer, R.; Berthon-Fabry, S. Tin dioxide coated carbon materials as an alternative catalyst support for PEMFCs: Impacts of the intrinsic carbon properties and the synthesis parameters on the coating characteristics. *Microporous Mesoporous Mater.* **2018**, *271*, 1–15. [CrossRef]
15. Asset, T.; Chattot, R.; Maillard, F.; Dubau, L.; Ahmad, Y.; Batisse, N.; Dubois, M.; Guérin, K.; Labbé, F.; Metkemeijer, R.; et al. Activity and Durability of Platinum-Based Electrocatalysts Supported on Bare or Fluorinated Nanostructured Carbon Substrates. *J. Electrochem. Soc.* **2018**, *165*, F3346–F3358. [CrossRef]
16. Sahoo, M.; Scott, K.; Ramaprabhu, S. Platinum decorated on partially exfoliated multiwalled carbon nanotubes as high performance cathode catalyst for PEMFC. *Int. J. Hydrogen Energy* **2015**, *40*, 9435–9443. [CrossRef]
17. Wang, Y.; Jin, J.; Yang, S.; Li, G.; Qiao, J. Highly active and stable platinum catalyst supported on porous carbon nanofibers for improved performance of PEMFC. *Electrochim. Acta* **2015**, *177*, 181–189. [CrossRef]
18. Singh, R.; Singh, M.K.; Bhartiya, S.; Singh, A.; Kohli, D.K.; Ghosh, P.C.; Meenakshi, S.; Gupta, P.K. Facile synthesis of highly conducting and mesoporous carbon aerogel as platinum support for PEM fuel cells. *Int. J. Hydrogen Energy* **2017**, *42*, 11110–11117. [CrossRef]
19. Yadav, R.; Subhash, A.; Chemmenchery, N.; Kandasubramanian, B. Graphene and graphene oxide for fuel cell technology. *Ind. Eng. Chem. Res.* **2018**, *57*, 9333–9350. [CrossRef]
20. Grigoriev, S.A.; Fateev, V.N.; Pushkarev, A.S.; Pushkareva, I.V.; Ivanova, N.A.; Kalinichenko, V.N.; Presnyakov, M.Y.; Wei, X. Reduced Graphene Oxide and Its Modifications as Catalyst Supports and Catalyst Layer Modifiers for PEMFC. *Materials (Basel)* **2018**, *11*, 1405. [CrossRef]
21. Işıkel Şanlı, L.; Bayram, V.; Ghobadi, S.; Düzen, N.; Alkan Gürsel, S. Engineered catalyst layer design with graphene-carbon black hybrid supports for enhanced platinum utilization in PEM fuel cell. *Int. J. Hydrogen Energy* **2017**, *42*, 1085–1092. [CrossRef]
22. Marinoiu, A.; Carcadea, E.; Sacca, A.; Carbone, A.; Sisu, C.; Dogaru, A.; Raceanu, M.; Varlam, M. One-step synthesis of graphene supported platinum nanoparticles as electrocatalyst for PEM fuel cells. *Int. J. Hydrogen Energy* **2020**, *45*. [CrossRef]
23. Pushkarev, A.S.; Alekseeva, O.K.; Pushkareva, I.V.; Shapir, B.L.; Chumakov, R.G.; Tishkin, V.V.; Kozlova, M.V.; Kalinichenko, V.N.; Fateev, V.N. Plasma doping of nanostructed reduced graphene oxide. *Nanotechnol. Russ.* **2020**, *3–6*. in press.
24. Erickson, K.; Erni, R.; Lee, Z.; Alem, N.; Gannett, W.; Zettl, A. Determination of the Local Chemical Structure of Graphene Oxide and Reduced Graphene Oxide. *Adv. Mater.* **2010**, *22*, 4467–4472. [CrossRef] [PubMed]
25. Du, L.; Shao, Y.; Sun, J.; Yin, G.; Liu, J.; Wang, Y. Advanced catalyst supports for PEM fuel cell cathodes. *Nano Energy* **2016**, *29*, 314–322. [CrossRef]

26. Liu, M.; Zhang, R.; Chen, W. Graphene-Supported Nanoelectrocatalysts for Fuel Cells: Synthesis, Properties, and Applications. *Chem. Rev.* **2014**, *114*, 5117–5160. [CrossRef]
27. Pandey, R.P.; Shukla, G.; Manohar, M.; Shahi, V.K. Graphene oxide based nanohybrid proton exchange membranes for fuel cell applications: An overview. *Adv. Colloid Interface Sci.* **2017**, *240*, 15–30. [CrossRef]
28. Soo, L.T.; Loh, K.S.; Mohamad, A.B.; Daud, W.R.W.; Wong, W.Y. An overview of the electrochemical performance of modified graphene used as an electrocatalyst and as a catalyst support in fuel cells. *Appl. Catal. A Gen.* **2015**, *497*, 198–210. [CrossRef]
29. Alekseeva, O.K.; Pushkareva, I.V.; Pushkarev, A.S.; Fateev, V.N. Graphene and Graphene-Like Materials for Hydrogen Energy. *Nanotechnol. Russ.* **2020**, *15*, 273–300. [CrossRef]
30. Pak Hoe, L.; Boaventura, M.; Lagarteira, T.; Kee Shyuan, L.; Mendes, A. Polyol synthesis of reduced graphene oxide supported platinum electrocatalysts for fuel cells: Effect of Pt precursor, support oxidation level and pH. *Int. J. Hydrogen Energy* **2018**, *43*, 16998–17011. [CrossRef]
31. Daş, E.; Alkan Gürsel, S.; Işıkel Şanlı, L.; Bayrakçeken Yurtcan, A. Thermodynamically controlled Pt deposition over graphene nanoplatelets: Effect of Pt loading on PEM fuel cell performance. *Int. J. Hydrogen Energy* **2017**. [CrossRef]
32. Şanlı, L.I.; Bayram, V.; Yarar, B.; Ghobadi, S.; Gürsel, S.A. Development of graphene supported platinum nanoparticles for polymer electrolyte membrane fuel cells: Effect of support type and impregnation–reduction methods. *Int. J. Hydrogen Energy* **2016**, *41*, 3414–3427. [CrossRef]
33. Daş, E.; Alkan Gürsel, S.; Işikel Şanli, L.; Bayrakçeken Yurtcan, A. Comparison of two different catalyst preparation methods for graphene nanoplatelets supported platinum catalysts. *Int. J. Hydrogen Energy* **2016**, *41*, 9755–9761. [CrossRef]
34. Marinkas, A.; Arena, F.; Mitzel, J.; Prinz, G.M.; Heinzel, A.; Peinecke, V.; Natter, H. Graphene as catalyst support: The influences of carbon additives and catalyst preparation methods on the performance of PEM fuel cells. *Carbon N. Y.* **2013**, *58*, 139–150. [CrossRef]
35. Hsieh, S.H.; Hsu, M.C.; Liu, W.L.; Chen, W.J. Study of Pt catalyst on graphene and its application to fuel cell. *Appl. Surf. Sci.* **2013**, *277*, 223–230. [CrossRef]
36. Kim, S.-H.; Jeong, G.H.; Choi, D.; Yoon, S.; Jeon, H.B.; Lee, S.-M.; Kim, S.-W. Synthesis of noble metal/graphene nanocomposites without surfactants by one-step reduction of metal salt and graphene oxide. *J. Colloid Interface Sci.* **2013**, *389*, 85–90. [CrossRef]
37. Xin, Y.; Liu, J.; Zhou, Y.; Liu, W.; Gao, J.; Xie, Y.; Yin, Y.; Zou, Z. Preparation and characterization of Pt supported on graphene with enhanced electrocatalytic activity in fuel cell. *J. Power Sources* **2011**, *196*, 1012–1018. [CrossRef]
38. Hsin, Y.L.; Hwang, K.C.; Yeh, C.-T. Poly(vinylpyrrolidone)-Modified Graphite Carbon Nanofibers as Promising Supports for PtRu Catalysts in Direct Methanol Fuel Cells. *J. Am. Chem. Soc.* **2007**, *129*, 9999–10010. [CrossRef]
39. Antolini, E. Graphene as a new carbon support for low-temperature fuel cell catalysts. *Appl. Catal. B Environ.* **2012**, *123–124*, 52–68. [CrossRef]
40. Yang, Z.; Ball, S.; Condit, D.; Gummalla, M. Systematic Study on the Impact of Pt Particle Size and Operating Conditions on PEMFC Cathode Catalyst Durability. *J. Electrochem. Soc.* **2011**, *158*, B1439. [CrossRef]
41. Xu, Z.; Zhang, H.; Zhong, H.; Lu, Q.; Wang, Y.; Su, D. Effect of particle size on the activity and durability of the Pt/C electrocatalyst for proton exchange membrane fuel cells. *Appl. Catal. B Environ.* **2012**, *111–112*, 264–270. [CrossRef]
42. Avcioglu, G.S.; Ficicilar, B.; Eroglu, I. Effect of PTFE nanoparticles in catalyst layer with high Pt loading on PEM fuel cell performance. *Int. J. Hydrogen Energy* **2016**, *41*, 10010–10020. [CrossRef]
43. Mukerjee, S.; Srinivasan, S.; Appleby, A.J. Effect of sputtered film of platinum on low platinum loading electrodes on electrode kinetics of oxygen reduction in proton exchange membrane fuel cells. *Electrochim. Acta* **1993**, *38*, 1661–1669. [CrossRef]
44. Avcioglu, G.S.; Ficicilar, B.; Eroglu, I. Effective factors improving catalyst layers of PEM fuel cell. *Int. J. Hydrogen Energy* **2018**, *43*, 10779–10797. [CrossRef]
45. Ye, L.; Gao, Y.; Zhu, S.; Zheng, J.; Li, P.; Zheng, J.P. A Pt content and pore structure gradient distributed catalyst layer to improve the PEMFC performance. *Int. J. Hydrogen Energy* **2017**, *42*, 7241–7245. [CrossRef]
46. Schneider, C.A.; Rasband, W.S.; Eliceiri, K.W. NIH Image to ImageJ: 25 years of image analysis. *Nat. Methods* **2012**, *9*, 671–675. [CrossRef]
47. Alam, S.N.; Sharma, N.; Kumar, L. Synthesis of Graphene Oxide (GO) by Modified Hummers Method and Its Thermal Reduction to Obtain Reduced Graphene Oxide (rGO). *Graphene* **2017**, *6*, 1–18. [CrossRef]
48. Sharma, S.; Ganguly, A.; Papakonstantinou, P.; Miao, X.; Li, M.; Hutchison, J.L.; Delichatsios, M.; Ukleja, S. Rapid Microwave Synthesis of CO Tolerant Reduced Graphene Oxide-Supported Platinum Electrocatalysts for Oxidation of Methanol. *J. Phys. Chem. C* **2010**, *114*, 19459–19466. [CrossRef]
49. Jung, D.; Balamurugan, J.; Kim, N.H.; Lee, S.H.; Bhattacharyya, D.; Lee, J.H. Facile fabrication of highly durable Pt NPs/3D graphene hierarchical nanostructure for proton exchange membrane fuel cells. *Carbon N. Y.* **2016**, *109*, 805–812. [CrossRef]
50. Walton, J.; Wincott, P.; Fairley, N.; Carrick, A. *Peak fitting with CasaXPS: A Casa Pocket Book*; Accolyte Science: Knutsford, UK, 2010.
51. Naumkin, A.V.; Kraut-Vass, A.; Powell, C.J.; Gaarenstroom, S. NIST Standard Reference Database 20 version 4.1. Last Updated: 15 September 2012. Available online: https://srdata.nist.gov/xps/Default.aspx (accessed on 11 February 2021).
52. Aricò, A.S.; Shukla, A.K.; Kim, H.; Park, S.; Min, M.; Antonucci, V. An XPS study on oxidation states of Pt and its alloys with Co and Cr and its relevance to electroreduction of oxygen. *Appl. Surf. Sci.* **2001**, *172*, 33–40. [CrossRef]

53. Ma, J.; Habrioux, A.; Luo, Y.; Ramos-Sanchez, G.; Calvillo, L.; Granozzi, G.; Balbuena, P.B.; Alonso-Vante, N. Electronic interaction between platinum nanoparticles and nitrogen-doped reduced graphene oxide: Effect on the oxygen reduction reaction. *J. Mater. Chem. A* **2015**, *3*, 11891–11904. [CrossRef]
54. Yarar Kaplan, B.; Haghmoradi, N.; Biçer, E.; Merino, C.; Alkan Gürsel, S. High performance electrocatalysts supported on graphene based hybrids for polymer electrolyte membrane fuel cells. *Int. J. Hydrogen Energy* **2018**, *43*, 23221–23230. [CrossRef]
55. Gasteiger, H.A.; Kocha, S.S.; Sompalli, B.; Wagner, F.T. Activity benchmarks and requirements for Pt, Pt-alloy, and non-Pt oxygen reduction catalysts for PEMFCs. *Appl. Catal. B Environ.* **2005**, *56*, 9–35. [CrossRef]
56. Li, Y.; Tang, L.; Li, J. Preparation and electrochemical performance for methanol oxidation of pt/graphene nanocomposites. *Electrochem. Commun.* **2009**, *11*, 846–849. [CrossRef]
57. Avcioglu, G.S.; Ficicilar, B.; Bayrakceken, A.; Eroglu, I. High performance PEM fuel cell catalyst layers with hydrophobic channels. *Int. J. Hydrogen Energy* **2015**, *40*, 7720–7731. [CrossRef]
58. Prabhuram, J.; Zhao, T.; Wong, C.; Guo, J. Synthesis and physical/electrochemical characterization of Pt/C nanocatalyst for polymer electrolyte fuel cells. *J. Power Sources* **2004**, *134*, 1–6. [CrossRef]
59. Schmidt, T.J.; Gasteiger, H.A.; Stab, G.D.; Urban, P.M.; Kolb, D.M.; Behm, R.J. Characterization of High-Surface-Area Electrocatalysts Using a Rotating Disk Electrode Configuration. *J. Electrochem. Soc.* **1998**, *145*, 2354–2358. [CrossRef]
60. Hara, M.; Lee, M.; Liu, C.H.; Chen, B.H.; Yamashita, Y.; Uchida, M.; Uchida, H.; Watanabe, M. Electrochemical and Raman spectroscopic evaluation of Pt/graphitized carbon black catalyst durability for the start/stop operating condition of polymer electrolyte fuel cells. *Electrochim. Acta* **2012**, *70*, 171–181. [CrossRef]
61. Speder, J.; Zana, A.; Spanos, I.; Kirkensgaard, J.J.K.; Mortensen, K.; Hanzlik, M.; Arenz, M. Comparative degradation study of carbon supported proton exchange membrane fuel cell electrocatalysts—The influence of the platinum to carbon ratio on the degradation rate. *J. Power Sources* **2014**, *261*, 14–22. [CrossRef]
62. Pizzutilo, E.; Geiger, S.; Grote, J.-P.; Mingers, A.; Mayrhofer, K.J.J.; Arenz, M.; Cherevko, S. On the Need of Improved Accelerated Degradation Protocols (ADPs): Examination of Platinum Dissolution and Carbon Corrosion in Half-Cell Tests. *J. Electrochem. Soc.* **2016**, *163*, F1510–F1514. [CrossRef]
63. Zhang, Y.; Chen, S.; Wang, Y.; Ding, W.; Wu, R.; Li, L.; Qi, X.; Wei, Z. Study of the degradation mechanisms of carbon-supported platinum fuel cells catalyst via different accelerated stress test. *J. Power Sources* **2015**, *273*, 62–69. [CrossRef]
64. Dubau, L.; Castanheira, L.; Maillard, F.; Chatenet, M.; Lottin, O.; Maranzana, G.; Dillet, J.; Lamibrac, A.; Perrin, J.-C.; Moukheiber, E.; et al. A review of PEM fuel cell durability: Materials degradation, local heterogeneities of aging and possible mitigation strategies. *Wiley Interdiscip. Rev. Energy Environ.* **2014**, *3*, 540–560. [CrossRef]
65. Yu, K.; Groom, D.J.; Wang, X.; Yang, Z.; Gummalla, M.; Ball, S.C.; Myers, D.J.; Ferreira, P.J. Degradation Mechanisms of Platinum Nanoparticle Catalysts in Proton Exchange Membrane Fuel Cells: The Role of Particle Size. *Chem. Mater.* **2014**, *26*, 5540–5548. [CrossRef]
66. Sharma, R.; Andersen, S.M. An opinion on catalyst degradation mechanisms during catalyst support focused accelerated stress test (AST) for proton exchange membrane fuel cells (PEMFCs). *Appl. Catal. B Environ.* **2018**, *239*, 636–643. [CrossRef]
67. Devrim, Y.; Arıca, E.D.; Albostan, A. Graphene based catalyst supports for high temperature PEM fuel cell application. *Int. J. Hydrogen Energy* **2018**. [CrossRef]
68. Bharti, A.; Cheruvally, G. Influence of various carbon nano-forms as supports for Pt catalyst on proton exchange membrane fuel cell performance. *J. Power Sources* **2017**, *360*, 196–205. [CrossRef]
69. Zhao, Z.; Castanheira, L.; Dubau, L.; Berthomé, G.; Crisci, A.; Maillard, F. Carbon corrosion and platinum nanoparticles ripening under open circuit potential conditions. *J. Power Sources* **2013**, *230*, 236–243. [CrossRef]
70. Castanheira, L.; Dubau, L.; Mermoux, M.; Berthomé, G.; Caqué, N.; Rossinot, E.; Chatenet, M.; Maillard, F. Carbon Corrosion in Proton-Exchange Membrane Fuel Cells: From Model Experiments to Real-Life Operation in Membrane Electrode Assemblies. *ACS Catal.* **2014**, *4*, 2258–2267. [CrossRef]
71. Shaari, N.; Kamarudin, S.K. Graphene in electrocatalyst and proton conductiong membrane in fuel cell applications: An overview. *Renew. Sustain. Energy Rev.* **2017**, *69*, 862–870. [CrossRef]
72. Baranov, I.E.; Grigoriev, S.A.; Ylitalo, D.; Fateev, V.N.; Nikolaev, I. Transfer processes in PEM fuel cell: Influence of electrode structure. *Int. J. Hydrogen Energy* **2006**, *31*, 203–210. [CrossRef]
73. Grigoriev, S.A.; Millet, P.; Fateev, V.N. Evaluation of carbon-supported Pt and Pd nanoparticles for the hydrogen evolution reaction in PEM water electrolysers. *J. Power Sources* **2008**, *177*, 281–285. [CrossRef]
74. Pushkarev, A.S.; Pushkareva, I.V.; Ivanova, N.A.; Du Preez, S.P.; Bessarabov, D.; Chumakov, R.G.; Stankevich, V.G.; Fateev, V.N.; Evdokimov, A.A.; Grigoriev, S.A. Pt/C and Pt/SnOx/C catalysts for ethanol electrooxidation: Rotating disk electrode study. *Catalysts* **2019**, *9*. [CrossRef]
75. Pushkarev, A.S.; Pushkareva, I.V.; Akelkina, S.V.; Kozlova, M.V.; Grigoriev, S.A.; Kuleshov, N.V.; Bessarabov, D.G. Electrocatalytic materials for solid polymer electrolyte water electrolyzers. *J. Phys. Conf. Ser.* **2020**, *1683*, 052022. [CrossRef]
76. Grigor'ev, S.A.; Lyutikova, E.K.; Pritulenko, E.G.; Samsonov, D.P.; Fateev, V.N. Synthesis and test of palladium-based nanostructured anodic electrocatalysts for hydrogen fuel cells with solid polymer electrolyte. *Russ. J. Electrochem.* **2006**, *42*, 1251–1254. [CrossRef]
77. Pushkarev, A.S.; Pushkareva, I.V.; Solovyev, M.A.; Butrim, S.I.; Grigoriev, S.A. The study of the solid polymer electrolyte oxygen concentrator with nanostructural catalysts based on hydrophobized support. *Nanotechnol. Russ.* **2020**, *3–6*, in press.

78. Sassin, M.B.; Garsany, Y.; Gould, B.D.; Swider-Lyons, K.E. Fabrication Method for Laboratory-Scale High-Performance Membrane Electrode Assemblies for Fuel Cells. *Anal. Chem.* **2017**, *89*, 511–518. [CrossRef]
79. Atkinson, R.W.; Garsany, Y.; Gould, B.D.; Swider-Lyons, K.E.; Zenyuk, I.V. The Role of Compressive Stress on Gas Diffusion Media Morphology and Fuel Cell Performance. *ACS Appl. Energy Mater.* **2018**, *1*, 191–201. [CrossRef]